High Resolution Airborne Infrared Measurements of Ocean Skin Temperature

Christopher J. Zappa, *Member, IEEE*, and Andrew T. Jessup, *Member, IEEE*

***Abstract*— Airborne measurements of ocean skin temperature, T_s, are presented from the Coupled Boundary Layers, Air-Sea Transfer in Low Winds (CBLAST-Low) Pilot Experiment in August 2001 off Martha's Vineyard, MA. We used an infrared (IR) camera with a spatial resolution of 1 m or less and temperature resolution of roughly 0.02°C. Using sub-frame sampling of the IR imagery, we achieve lower noise and higher spatial resolution than reported by previous investigators using IR radiometers. Fine-scale maps of T_s exhibit horizontal variability over spatial scales ranging from *O*(10 km) down to *O*(1 m) that are related to atmospheric and sub-surface phenomena under low to moderate wind conditions. Based on supporting measurements of wind and waves, we identify coherent ramp-like structures in T_s with stratification breakdown and meandering streaky features with internal waves. Regional maps of T_s show the standard deviation for the region is ±1.04°C while the meridional and zonal variability is 0.23°C km^{-1} and 0.27°C km^{-1}, respectively. This temperature variability results in meridional and zonal scalar heat flux variability of 7.0 W m^{-2} km^{-1} and 7.6 W m^{-2} km^{-1}, respectively. Our results demonstrate the potential for airborne IR imagery accompanied by high-quality ocean data to identify T_s features produced by subsurface circulation.**

***Index Terms*—Airborne infrared imaging, ocean skin temperature, air-sea interaction, upper ocean processes, internal waves.**

I. Introduction

RESULTS from the Tropical Ocean-Global Atmosphere, Coupled Ocean-Atmosphere Response Experiment (TOGA-COARE) have demonstrated the importance of ocean skin temperature, T_s, in air-sea interaction. Accurate knowledge of T_s has been shown to be critical to estimating surface fluxes [1] and as a result its spatial variability influences the small-scale distribution of those fluxes [2], [3]. The focus of our observations is the spatial variability of T_s under low wind conditions.

Results reported by *Hagan et al.* [2] were derived from airborne measurements made with a narrow field-of-view (FOV) infrared (IR) radiometer. They reported an effective spatial resolution of 100 m with a resulting temperature resolution of 0.1°C. For wind speeds less than 4 m s^{-1}, they found diurnal warming of the skin layer that preceded subsequent increases in subsurface temperature. Horizontal gradients of 1°C in 10 km were observed under conditions of low wind and high solar insolation. *Walsh et al.* [3] reported on concurrent measurements from a different aircraft that included mean square wave slope. They observed horizontal variability in T_s on 5-km scales that was anticorrelated with the slope. The patterns propagated with a speed and direction that was similar to internal gravity waves detected by moorings. They suggested that coupling between the internal waves and the diurnal surface layer might be responsible for their observations, which implies that subsurface temperature patterns penetrate into the skin layer.

Early demonstration of the potential of IR imagery of the ocean surface from aircraft were reported by *McAlister and McLeish* [4] and *McLeish* [5], [6]. They performed some of the first measurements of the horizontal structure of T_s using an IR scanner and recorded signatures of apparent fronts, large-scale ocean eddies, free-convective patterns, wind streaks, surface slicks, and whitecapping. However, there were no upper ocean measurements to corroborate the processes responsible for the IR signatures. Furthermore, the scanned IR images show indications of significant fixed pattern noise and were not corrected for sky reflection. *Peltzer et al.* [7] used an airborne IR imaging system for the detection of ship wakes during the day, when the diurnal thermocline was well established. The thermal wake signatures recorded by the imaging system depict the contrast between the cool center of the ship wake produced by the upwelling of the underlying water and a warmer undisturbed surface layer.

Marmorino et al. [8] have also recently reported airborne measurements with an IR imager showing distinctive banding structures in T_s under low wind speed conditions. They found that the temperature patterns propagated in a manner similar to those of internal waves found in SAR imagery and present evidence for thinning of the cool skin layer by straining due to internal wave currents. They concluded that the streaky features they observed were likely the IR signature of internal waves, although no *in-situ* measurements confirming the presence of internal waves was available.

Here, we report on the spatial variability of T_s using airborne IR measurements during the field campaign of the

Manuscript received February 27, 2004; revised July 13, 2004. This work was funded by the U.S. Office of Naval Research under Grant No. N00014-01-1-0081 (Zappa) and Grant No. N00014-01-1-0080 (Jessup).

C. J. Zappa was with the Woods Hole Oceanographic Institution, Woods Hole, MA 02543 USA. He is now with the Lamont-Doherty Earth Observatory, Columbia University, Palisades, NY 10964 USA (phone: 845-365-8547; fax: 845-365-8157; e-mail: zappa@ldeo.columbia.edu).

A. T. Jessup is with the Applied Physics Laboratory, University of Washington, Seattle, WA 98105 USA. (e-mail: jessup@apl.washington.edu).

Coupled Boundary Layers, Air-Sea Transfer in Low Winds (CBLAST-Low) Pilot Experiment in August 2001. The airborne measurements were made in conjunction with detailed *in-situ* measurements of wind, waves, subsurface temperature, and currents. The extensive spatial coverage and fine spatial and temperature resolution of our systems allows us to examine spatial scales in T_s from processes that span the atmospheric boundary layer of O(1km) down to wave-related processes O(1m). We produced thermal maps of the study site using spatial series of T_s and compared these with the fine-scale structures observed within the IR imagery to investigate a variety of processes with varying scales in the coastal zone. We combine the airborne IR data with upper ocean measurements to relate horizontal variability in T_s to sub-surface phenomena. Our results demonstrate the significance of the T_s spatial variability for regional heat flux estimation as well as the value of combining high resolution IR imagery with *in-situ* measurements.

II. Experiment

The CBLAST-Low study site was off the south coast of Martha's Vineyard, MA and covered a rectangular region of roughly 40 km along the south shore and 50 km offshore. Our instrumentation was flown on the LongEZ [9] operated by the National Oceanic and Atmospheric Administration Air Resources Laboratory. The flights occurred on days with light to moderate winds (< 10 m s^{-1}) under a variety of atmospheric stability conditions. The flights considered here were made before/near sunrise or near/after sunset and at the nominal altitude of roughly 400 m with occasional flights at lower altitudes down to 100 m. *In-situ* measurements of meteorological and wave conditions were made at the Martha's Vineyard Coastal Observatory (MVCO), which includes the South Beach meteorological mast and a subsurface node mounted in 12-m water depth approximately 1.5 km offshore. The SecNav and CBLAST surface moorings, located in 27 m and 47 m water depth, respectively, provided high-resolution temperature, salinity, and velocity measurements throughout the water column as well as surface meteorological data [10]. The flight surveys quantified the horizontal mesoscale variability in T_s from the coast to the CBLAST surface mooring 40 km offshore, as well as utilized the *in-situ* data sets to directly compare sea-surface IR signatures with the oceanic surface layer processes and atmospheric boundary layer fluxes.

Airborne measurements of T_s were made using two complimentary IR sensors. A model Radiance HS IR imager (Amber Engineering, Goleta, CA) containing a 256x256 element focal-plane detector array operating over 3-5 μm provided high spatial and temporal resolution imagery. A model KT-15 narrow FOV radiometer (Heitronics, Wiesbaden, Germany) operating over 8-14 μm provided calibrated T_s at lower resolution. A sky correction was implemented [11] with an upward-looking model 4000GL narrow FOV radiometer (Everest Interscience Inc., Tucson, AZ). A downward-looking model 9701 digital video camera (Pulnix America Inc., Sunnyvale, CA) was also used. Prior to each flight, the IR imagery was corrected for non-uniformity and calibrated using a model 2004S blackbody (Santa Barbara Infrared Inc., Santa Barbara, CA). The KT-15 radiometer was calibrated pre- and post- experiment in the laboratory and was used to calibrate the IR imagery.

The IR imager was operated concurrently in two distinct modes identified as Full Frame and Sub-Frame (Averaged) mode. In the Full Frame mode, complete images acquired at 1 Hz provided an instantaneous 2-D map of T_s with spatial resolution of less than 1 m and thermal resolution of roughly 0.02°C. In the Sub-Frame mode, point measurements were made by taking the average of a subset of each image (3x3, 16x17, and 256x256) at a frame rate of 30 Hz. Since each subset of N pixels can be regarded as N independent measurements, averaging the values within a subset will reduce the noise by a factor $1/\sqrt{N}$. This averaging technique increases the signal-to-noise ratio (SNR) while retaining a fast sample rate. In Sub-Frame mode with the 3x3 subset, the imager provided a "spot" measurement of T_s with a temperature resolution of less than 0.02°C and a spatial resolution of O(1m).

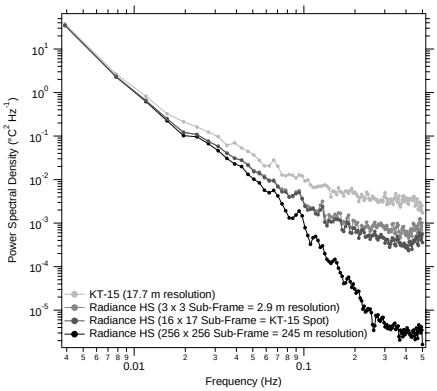

Fig. 1. Spectra for T_s for the radiometer (17.7 m resolution) and three imager subsets in Sub-Frame mode (2.9 m, 17.7 m, and 245 m resolution).

III. Results

The Sub-Frame mode technique provides lower noise and higher spatial resolution than can be obtained using IR radiometers, which require significant temporal averaging that reduces spatial resolution when operated from aircraft. Figure 1 shows power spectra for T_s comparing the IR radiometer to the three sub-frame resolutions for the IR imager. These data were taken at night on 3 August, 2001 from about 0100 - 0300 UTC (local = UTC - 4 hours) when the wind speed ranged from 6 to 10 m s^{-1} and the direction was from the SW. At the altitude of 389 m, the spatial resolution for the radiometer was 17.7 m. The effective spatial resolution for the imager subsets is 2.9 m, 17.7 m (IR radiometer resolution), and 245 m. The noise floor for the IR radiometer is an order of magnitude higher than that for the IR imager in Sub-Frame mode with the identical spatial resolution. The noise-equivalent temperature difference for the radiometer is greater than 0.15°C, while that

of the imager is less than 0.01°C. In cases when spatial resolution is crucial, the noise floor for the imager in Sub-Frame mode at the finer resolution of 2.9 m was still nearly an order of magnitude lower than the radiometer. In cases when high spatial resolution is not required, using the full image in Sub-Frame mode (245 m resolution) reduced the noise floor to nearly 3 orders of magnitude below that of the radiometer. The observed SNR for the three subset matrices was of the same order as the theoretical SNR. These results confirm that the Sub-Frame mode provides higher spatial resolution and lower noise than can be achieved using radiometers from aircraft.

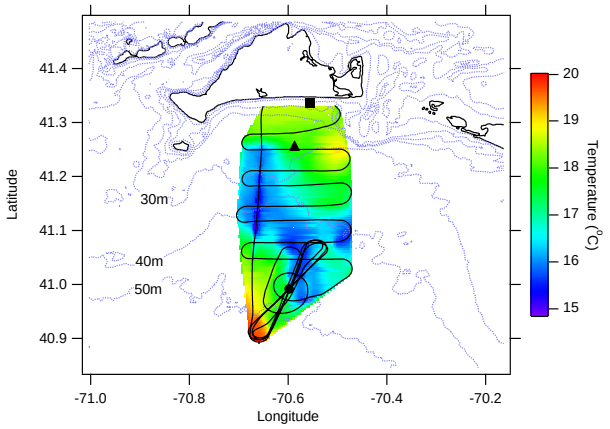

Fig. 2. Typical map of T_s from the imager in Sub-Frame mode. The black trace is the flight track and the symbols show the MVCO subsurface node (■; 41° 20.2' N, 70° 33.4' W), and the SecNav (▲; 41° 15.4' N, 70° 35.2' W) and CBLAST (●; 40° 59.5' N, 70° 35.8' W) surface mooring.

An interpolated map of T_s produced using a standard triangulation algorithm on the Sub-Frame data is shown in Figure 2. The data were taken at dawn on 31 July, 2001 from 0930 - 1200 UTC from an altitude of 390 m. The wind speed ranged from 4 to 6 m s^{-1} during this flight and the direction was from the NE. The example in Figure 2 is typical for the 2001 pilot study and shows large-scale spatial variability of several degrees over 10 km. Two quantitative measures of this variability in T_s are its standard deviation and the root-mean-square (RMS) of its spatial derivative. The standard deviation for the region is ±1.04°C while the RMS derivatives are 0.23°C km^{-1} and 0.27°C km^{-1} for the meridional (North-South) and the zonal (East-West), respectively. The horizontal gradients of more than a 2°C change in 10 km observed here are significantly greater than those observed in the equatorial Pacific over the same spatial scales [2].

One of the goals of CBLAST-Low was to examine the influence of spatial variability of T_s on the regional heat flux variability and the development of transfer coefficient relationships. Skin temperature variability is important to the regional estimates of heat fluxes extrapolated from individual locations since regional flux estimates require an accuracy of better than 10 W m^{-2} [1]. The spatial heat flux variability is also important to modeling the heat transfer coefficients since the spatial variability of the region is integrated into direct covariance flux measurements [12]. The integrated area that effects the covariance fluxes, or the flux footprint, is dependent on the development of the boundary layer height and wind speed and is typically of O(1-10 km).

We estimated the heat flux variability due to T_s alone by implementing the TOGA COARE algorithm for the scalar fluxes. The standard expressions for the sensible and latent scalar heat fluxes are

$$Q_s = \rho_a c_p C_h U_{10}(\theta - T_s)$$
$$Q_l = \rho_a L_e C_e U_{10}(q - q_s) \quad (1)$$

where ρ_a is the density of air, c_p is the specific heat of air, U_{10} is the wind speed at 10 m, θ is the potential air temperature, L_e is the latent heat of vaporization, q is the water vapor mixing ratio, and q_s is the interfacial value of the water vapor mixing ratio that is computed from the saturation mixing ratio for pure water at T_s. The transfer coefficients for sensible and latent heat, C_h and C_e, are nonlinear and calculated using the TOGA-COARE model [1]. The model input parameters (U_{10}, q, θ) were relatively uniform within the CBLAST-Low study site. The sum of the sensible and latent fluxes has been calculated according to (1) using the map of T_s in Figure 2 and the appropriate buoy data. The standard deviation in total scalar heat flux for the region under low wind speeds is ±31.4 W m^{-2}. The meridional scalar heat flux variability is 7.0 W m^{-2} km^{-1} and the zonal is 7.6 W m^{-2} km^{-1}. Therefore, these results suggest that the heat flux variability is dominated by T_s and will be crucial to accurately estimating the regional heat fluxes and to modeling the heat transfer coefficients.

Mechanisms that drive or enhance air-sea exchange under low wind speed conditions are suggested by small-scale structures that are apparent in the Full-Frame imagery. Figure 3a is an example of the IR signature that was observed during the passage of a discrete internal wave packet at the SecNav buoy site [10]. These data were taken at dawn on 1 August, 2001 from 1000 - 1230 UTC from an altitude of 190 m in the vicinity of 41° 11.4' N, 70° 34.8' W. The wind speed ranged from 2.2 to 3.2 m s^{-1} and the direction was from the NNW (see Figure 3b). The image is roughly 100 m by 100 m with a resolution roughly 0.4 m. Figure 3a shows distinctive banding streaks of various scales that are aligned with the bathymetry and perpendicular to both the wind and wave directions. Lighter shades of gray are warmer temperatures. These long parallel features exhibit an alternating thin cool region (roughly 1 to 5 m wide) followed by a broad warm region (roughly 20 to 35 m wide). Based on concurrent wind and wave measurements and coincident video imagery, it is unlikely that these features are due to surface gravity waves or Langmuir circulation. Wave data at the MVCO subsurface node show that the surface gravity waves, while propagating perpendicular to the streaks, had a dominant wavelength of 105 m, which is significantly greater than the streak spacing. The wind was perpendicular to the orientation of the streaks, making it unlikely that Langmuir circulation was the cause. Furthermore, coincident video imagery confirmed that the short-crested wind-wave direction was roughly perpendicular

to the orientation of the streaks. The streak orientation relative to the wind, waves and bathymetry imply that these band-like features observed are likely the surface manifestation of the internal waves of elevation observed to be propagating shoreward at the SecNav buoy site.

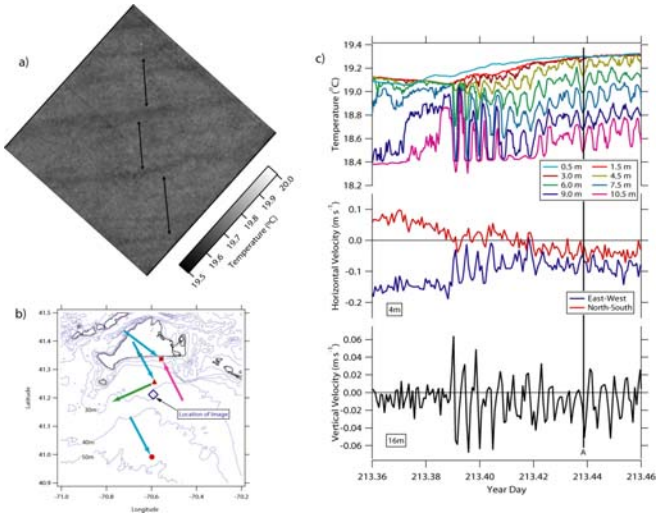

Fig. 3. (a) Example of banding features in IR imagery during the passage of internal waves. The arrows highlight the spacing of 20 m to 35 m between dark bands, which correspond to cooler temperature. (b) Map showing the location of the image in (a) and the directions of the wind (cyan), surface waves (magenta), and current (green) at the appropriate mooring site (see Figure 2 for key). Wind speed was 2.5 m s^{-1} from 307° at MVCO, 3.2 m s^{-1} from 331° at SecNav, and 2.2 m s^{-1} from 332° at CBLAST. The surface wave direction was from 156° with an 8.2 s period and height of 0.8 m measured at MVCO while the mean current at 4m depth measured at SecNav was 0.09 m s^{-1} to 246°. (c) Temperature and velocity time series measured at the SecNav buoy site showing the structures characteristic of the passage of internal waves. The time of the IR image is denoted in (c). The image scale is 100 m by 100 m (North is to the top of the page).

Internal tides generate interfacial waves of depression at the shelf break that propagate cross-shelf onshore into the CBLAST-Low region. The waves of depression shoal, break and transform into waves of elevation [13] that are observed in the SecNav buoy data [10]. In Figure 3c, subsurface temperatures from the SecNav subsurface vertical thermistor array show the evolution of a propagating internal wave train with peak to trough amplitude swings of nearly 0.7°C, or several meters in amplitude of isotherm excursion. Near-surface current meters demonstrate the existence of coherent variability in velocity, as shown in Figure 3c, indicating convergent/divergent zones that may modulate the small-scale surface roughness and/or accumulate surfactant as has been suggested by *Kropfli et al.* [14]. The streak spacing of 25 m to 40 m is consistent with the characteristic length scale of the internal waves estimated at the SecNav site to be roughly 30 m according to Korteweg-de Vries theory [10] and roughly 50 m from a separate three-dimensional mooring array deployed during this study [15].

The subsurface temperatures in Figure 3c indicate that the near-surface was well-mixed following an evening of cooling and small-scale overturning, and thus the temperature signature in the buoy data associated with the internal waves of elevation does not intrude into the top 3 m. Early work by *Osborne* [16] indicated that near-surface currents could modulate T_s by straining of the skin layer—thinning of the skin layer due to divergence leads to warmer regions and thickening due to convergence leads to cooler regions (assuming constant heat flux). *Marmorino et al.* [8] demonstrated that the magnitude of the observed T_s modulation was consistent with the strain rate that occurred for internal waves propagating within Tampa Bay. While the near surface here is observed to be well-mixed down to 3 m, measurements of the net interfacial heat flux (= 83.5 W m^{-2} out of the ocean; sum of latent, sensible, longwave, and solar heat fluxes across the skin layer [17]) demonstrate that a cool skin layer exists. Thus, the modulation of T_s of order 0.3°C in the IR imagery suggests that the internal waves cause surface straining of the cool skin layer by varying the near-surface convergent/divergent flow field. In addition to the straining of T_s by surface currents, the effect of accumulated surfactant may also contribute to the IR signature. To the best of our knowledge, these are the first such digital airborne IR images accompanied by high-quality *in-situ* data that indicate the direct modulation of T_s by internal waves.

We also observed the evolution of fine-scale features within the IR imagery during a nighttime transitional wind speed period. Figure 4 shows a comparison of IR imagery (a, b, c) taken before, during, and after the stratification breakdown that is demonstrated in the temperature time series (d) from the SecNav vertical thermistor array 9 km away. These IR data were taken at night on 3 August, 2001 from about 0100 - 0300 UTC from an altitude of 390 m in the vicinity of 41° 10.4' N, 70° 32.3' W. The wind speed was steadily increasing from 5 to 8 m s^{-1} and the direction was from the WSW. The images are roughly 245 m by 245 m with a spatial resolution roughly 1 m. The mean current was 36 cm s^{-1} to the SSE. Figure 4a shows a roughly uniform region of sea surface temperature and was taken when the upper ocean was well stratified (Yearday 215.02). As the wind-speed picked up,

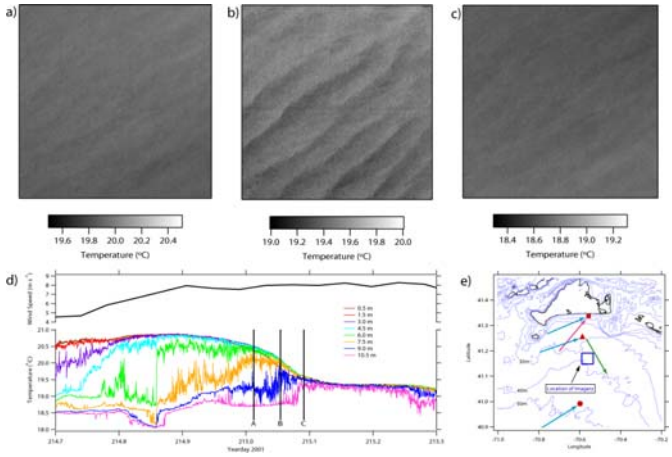

Fig. 4. IR images (a, b, c) showing the evolution of coherent ramp-like features observed on 3 August, 2001 stratification breakdown as indicated by wind speed and temperature (d). (e) Map showing location of the images in (a, b, c) and the directions of the wind, waves, and current (see Figure 2 for key). Wind speed was from 247°, 251°, 238° at MVCO, SecNav, and CBLAST, respectively. Wave direction was from 220° with a 4.4 s period and 1.1 m height at MVCO. Mean current at 4m depth at SecNav was 0.36 m s^{-1} to 150°. The times of the IR images are denoted in (d). The image scale is 245 m by 245 m (North is to the top of the page).

Figure 4b (Yearday 215.06) shows distinctive successive ramping features that steadily increase in temperature and abruptly drop by up to 0.5°C. These coincide with the complete near-surface layer mixing down to roughly 7.5 m and the ongoing abrupt mixing down to 9 m. The spatial scale of these coherent ramps structures is roughly 40 m, and the structures are oriented perpendicular to the current and roughly parallel to the wind and waves. Figure 4c (Yearday 215.09) shows a roughly uniform region of T_s and was taken following the abrupt mixing of the ocean down to 10.5 m.

These coherent ramp structures may be the IR signature of a mechanism in the near-surface layer that leads to the stratification breakdown under conditions when the turbulence transitions from a buoyancy- to a shear-driven state. *Soloviev* [18] has observed coherent ramp-like structures in a convectively unstable surface ocean where shear played an important role. *Thorpe* [19] observed similar coherent structures under stably stratified conditions as during CBLAST-Low and suggested that temperature ramps are likely due to large eddies with axes predominantly across-current caused by an instability in the shear flow. Our IR measurements demonstrate the ability to quantify these structures to determine their significance for the vertical fluxes of heat and momentum in the ocean.

The fine scale variability presented here is not resolved by satellite SST products, which have spatial resolution of roughly 1 km and 50 km for IR and passive microwave, respectively. When fluxes are estimated using sea surface temperature (SST) from satellites, the unresolved variability will degrade the accuracy of the flux estimate. The loss of accuracy is due to the non-linear dependence of the fluxes on the sea-air temperature difference. Specifically, the unresolved SST variability may lead to errors in the determination of the transfer coefficients where a satellite-averaged SST specifies a particular stability while the actual SST variability could specify both stable and unstable conditions. The unresolved SST variability may also lead to errors in the calculation of the specific humidity that evolve from the nonlinear Clausius-Clapeyron relationship. High-resolution airborne IR imagery in combination with *in-situ* measurements of heat flux can provide the means of assessing the magnitude of the error.

IV. Conclusions

The IR techniques presented can quickly characterize the spatial and temporal scales of a wide variety of processes that are important to the air-sea fluxes of heat, mass, and momentum. The results demonstrate the capability to provide T_s measurements with fine spatial (< 1 m) and temperature (0.02°C) resolution. The horizontal variability in the air-sea heat flux due to T_s alone has been shown to be at least 60 W m^{-2} over scales of 10 km. Internal waves propagating up the shelf produced band-like features in the IR imagery with temperature variability of 0.3°C and spatial scales of 25 to 40 m. Coherent ramp-like structures observed in the IR imagery with variability of 0.5°C and spatial scales of 40 m are likely due to stratification breakdown. Processes detectable using high-resolution IR imagery directly affect the thermal boundary layer and therefore are important to upper-ocean mixing, transport dynamics, and the magnitude and distribution of air-sea fluxes.

Acknowledgment

We thank G. Crescenti, M. Pritchard, and R. Weller for their contributions to this study. We dedicate this article to the late Tim Crawford. LDEO contribution No. 6696.

References

[1] C. W. Fairall, E. F. Bradley, D. P. Rogers, J. B. Edson, and G. S. Young, "Bulk parameterization of air-sea fluxes for Tropical Ocean Global Atmosphere Coupled Ocean Atmosphere Response Experiment," *J. Geophys. Res.*, vol. 101, pp. 3747-3764, 1996.

[2] D. Hagan, D. Rogers, C. Friehe, R. Weller, and E. Walsh, "Aircraft observations of sea surface temperature variability in the tropical pacific," *J. Geophys. Res.*, vol. 102, pp. 15733-15747, 1997.

[3] E. J. Walsh *et al.*, "Coupling of internal waves on the main thermocline to the diurnal surface layer and sea surface temperature during the Tropical Ocean-Global Atmosphere Coupled Ocean-Atmosphere Response Experiment," *J. Geophys. Res.*, vol. 103, pp. 12613-12628, 1998.

[4] E. D. McAlister and W. L. McLeish, "Oceanographic measurements with airborne infrared equipment and their limitations," in *Oceanography From Space*, G. C. Ewing, Ed. Woods Hole, MA: Woods Hole Oceanographic Inst. Rep. No. 65-10, 1965, pp. 189-215.

[5] W. McLeish, "On the mechanisms of wind-slick generation," *Deep-Sea Res.*, vol. 15, pp. 461-469, 1968.

[6] W. McLeish, "Spatial spectra of ocean surface temperature," *J. Geophys. Res.*, vol. 75, pp. 6872-6877, 1970.

[7] R. D. Peltzer, W. D. Garrett, and P. M. Smith, "A remote sensing study of a surface ship wake," *Int. J. Remote Sens.*, vol. 8, pp. 689-704, 1987.

[8] G. O. Marmorino, G. B. Smith, and G. J. Lindemann, "Infrared imagery of ocean internal waves," *Geophys. Res. Lett.*, vol. 31, pp. L11309, doi:10.1029/2004GL020152, 2004.

[9] T. L. Crawford, R. T. McMillen, T. P. Meyers, and B. B. Hicks, "Spatial and temporal variability of heat, water vapor, carbon dioxide, and momentum air-sea exchange in a coastal environmental," *J. Geophys. Res.*, vol. 98, pp. 12869-12880, 1993.

[10] M. Pritchard and R. A. Weller, "Observations of internal bores and waves of elevation on the New England inner continental shelf during summer 2001," *J. Geophys. Res.*, to be published.

[11] K. Katsaros, "Radiative sensing of sea surface temperature," in *Air Sea Interaction: Instruments and Methods*, F. Dobson, L. Hasse, and R. Davis, Eds. New York: Plenum Press, 1980, pp. 293-317.

[12] J. B. Edson, A. A. Hinton, K. E. Prada, J. E. Hare, and C. W. Fairall, "Direct covariance flux estimates from mobile platforms at sea," *J. Atmos. Oceanic Tech*, vol. 15, 1998.

[13] J. M. Klymak and J. N. Moum, "Internal solitary waves of elevation advancing on a shoaling shelf," *Geophys. Res. Lett.*, vol. 30, pp. 2045, doi:10.1029/2003GL017706, 2003.

[14] R. A. Kropfli *et al.*, "Relationships between strong internal waves in the coastal zone and their radar and radiometric signatures," *J. Geophys. Res.*, vol. 104, pp. 3133–3148, 1999.

[15] M. Pritchard and R. A. Weller, unpublished data.

[16] M. F. M. Osborne, "The effect of convergent and divergent flow patterns on infrared and optical radiation from the sea," *Deutsche Hydrographische Zeitschrift*, vol. 18, pp. 1-25, 1965.

[17] C. W. Fairall *et al.*, "Cool-skin and warm-layer effects on sea surface temperature," *J. Geophys. Res.*, vol. 101, pp. 1295-1308, 1996.

[18] A. V. Soloviev, "Coherent structures at the ocean surface in convectively unstable conditions," *Nature*, vol. 346, pp. 157-160, 1990.

[19] S. A. Thorpe, "The dynamics of the boundary layers of the deep ocean," *Science Progress*, vol. 72, pp. 189-206, 1988.